RSC Advances

PAPER

View Article Online
View Journal | View Issue

Cite this: *RSC Adv.*, 2022, **12**, 1043

Metal-free functionalized carbonized cotton for efficient solar steam generation and wastewater treatment†

Hiran D. Kiriarachchi,[a] Amr A. Hassan,[b] Fathi S. Awad *[c] and M. Samy El-Shall[a]

Water desalination *via* solar steam generation is one of the most important technologies to address the increasingly pressing global water scarcity. Materials for solar photothermal energy conversion are highly sought after for their cost savings, environmental friendliness and broad utility in many applications including domestic water heating and solar-driven desalination. Herein, we report the successful development of metal-free, low weight and cost effective functionalized carbonized cotton (CC) fibers for efficient solar water desalination and wastewater treatment. The CC fibers with nearly full solar spectrum absorption, efficient photo-thermal conversion and low-cost could provide excellent alternatives to the high-cost plasmonic-based materials for solar water desalination. We also report on a novel and simple device to mitigate the issues associated with conductive heat loss by utilizing the economically viable carbonized cotton materials as an irradiation surface placed on a low-density polyethylene foam that floats on the surface of seawater. The CC solar steam generation device exhibits average water evaporation rates of 0.9, 6.4 and 10.9 kg m^{-2} h^{-1} with impressive solar-to-vapor efficiencies of 59.2, 88.7 and 94.9% under 1, 5 and 8 sun illumination, respectively. Moreover, the device displays excellent durability showing stable evaporation rates over 10 steam generation cycles under 5 sun of solar intensity. Furthermore, the applicability of the CC device for the removal of organic dyes from contaminated water through solar steam generation is also demonstrated. The low-cost, simple design, high solar thermal evaporation efficiency, excellent stability and long-term durability make this CC device a perfect candidate for applications in seawater desalination and wastewater treatment by solar steam generation.

Received 17th November 2021
Accepted 20th December 2021

DOI: 10.1039/d1ra08438k

rsc.li/rsc-advances

Introduction

Seawater desalination *via* steam generation using sunlight is one of the most important technologies to address the increasingly pressing global water scarcity.[1–3] Therefore, solar steam generation has gained significant attention in recent years due to its important applications in seawater desalination,[4–12] wastewater treatment,[13] domestic water heating and even autoclave-based disinfection processes.[14] Due to the increasing energy demand and the environmental impact of fossil fuel consumption, it is essential to utilize abundant and clean renewable energy sources like solar energy in energy-yielding applications such as seawater desalination.

Materials used for solar photothermal energy conversion through heat localization are highly sought after for their cost savings, clean environmental impact and broad utility in providing water heating and/or steam for many applications including solar-driven desalination. Thus far, various materials have been utilized in fabricating steam generation devices such as metals,[3,4,15] metal oxides,[16,17] metal sulfides,[18] plasmonic metal nanoparticles,[7,8,19–22] and carbon-based composites.[12,23–27] However, bulk metals such as copper and aluminum have limited utility because of their inflexibility for tailored applications, high cost and limited availability.[3,4,15] Most important, these bulk metals are not very efficient in absorbing the solar spectrum and they exhibit significant heat loss through heat dissipation to bulk water. Also, the utility of plasmonic metal nanoparticles, although efficient, can be economically disadvantageous due to the high cost and complicated synthesis and processing.[7,8,20,21] On the contrary, carbon-based materials can be eco-friendly, low cost and energy efficient due to their low heat conductivity and most importantly they can absorb light in a wide wavelength range expanded over visible and near infrared (NIR) regions of solar spectrum.[23,24,28–34] Nevertheless, carbonized materials also possess several drawbacks including material shedding and poor mechanical properties,

[a]*Department of Chemistry, Virginia Commonwealth University, Richmond, VA 23284, USA*

[b]*Chemistry Department, Faculty of Science, Ain Shams University, Cairo 11566, Egypt*

[c]*Chemistry Department, Faculty of Science, Mansoura University, Mansoura 35516, Egypt. E-mail: fathyawad949@yahoo.com; Tel: +201000166374*

† Electronic supplementary information (ESI) available: Fig. S1 showing the experimental set up used for the solar steam generation experiments and Fig. S2 showing the solar evaporation data of CC and PC devices and DI water samples using a solar light density of 5 kW m^{-2}. See DOI: 10.1039/d1ra08438k

hydrophobicity with lack of wettability and porosity, and limited durability.

Herein, we report the successful development of metal-free, low weight and cost effective functionalized carbonized cotton (CC) fibers for efficient solar water desalination and wastewater treatment. We also report on a novel and simple device to mitigate the issues associated with conductive heat loss by utilizing the economically viable carbonized cotton materials as an irradiation surface placed on a low-density polyethylene foam that floats on the surface of seawater. This unique design allows the transfer of water by capillary forces through a cotton stalk to the external CC surface for solar thermal evaporation. Here, we demonstrate that the CC device can significantly enhance the conversion efficiency of sunlight into heat and solve some of the critical issues associated with the use of carbonized materials in solar steam generation such as material shedding, conductive heat loss and durability.

Materials and methods

Materials

Commercial cotton, nitric acid (50% w/w), low-density polyethylene foam, methylene blue.

Synthesis of functionalized carbonized cotton (CC)

Commercial cotton fibers were washed with deionized water to remove impurities followed by drying at 80 °C overnight. The dried cotton fibers were carbonized at 600 °C for several hours under an N_2 atmosphere to obtain the CC materials. To introduce hydrophilicity to the CC fibers, the materials were refluxed in a 50% HNO_3 solution at 80 °C for several hours. The resulting hydrophilic CC fibers were washed several times with deionized water followed by drying at 80 °C overnight.

Characterization

Pure cotton and CC fibers were characterized using a Nexus 670 FTIR spectrometer, (4 cm^{-1} resolution and 32 scans) using diamond attenuated total reflectance (DATR). The Raman spectrum of the CC fibers was measured using a Thermo Scientific DXR SmartRaman spectrometer (532 nm excitation). Surface structure and morphology of the pure and CC fibers were characterized using a Hitachi SU-70 FE-SEM scanning electron microscope (SEM). The optical characterization of the CC fibers was determined using a diffuse reflectance accessory attached to a Cary 6000i UV-vis-NIR spectrophotometer (Agilent Technologies). X-ray photoelectron spectroscopy (XPS) measurements of the CC fibers were conducted using a PHI VersaProbe III Scanning XPS Microprobe.

Solar steam generation experiments

A class ABA, Newport Sol2A, 450 W solar simulator was used to conduct the solar steam generation experiments. The experimental setup is shown in Fig. S1 (ESI†).[7,8] The solar steam generation rate of the CC device was measured under solar intensities of 1, 5 and 8 kW m^{-2}. Another device was prepared containing pure cotton fibers instead of the CC fibers as a control experiment. Solar intensities of 5 and 8 kW m^{-2} were obtained using a Fresnel lens (208.2 mm focal length and 279.4 mm diameter). In a typical steam generation experiment, the solar steam generation device was contained in a 100 mL beaker containing around 75 mL of water. The beaker was placed on a calibrated electronic balance. The temperatures of the evaporation surface and bulk water were measured using an IR heat sensor and a thermocouple, respectively. Normalized solar steam generation rates were calculated based on the weight loss of the water body per unit area of irradiation at a corresponding time interval (5 min). Normalized steam generation data were used to calculate the solar-to-vapor efficiency of the CC solar steam generation device. All the steam generation experiments were carried out at room temperature of 20 ± 1 °C and relative humidity of ~40%.

Wastewater treatment

To evaluate the applications of the CC steam generation device in wastewater treatment, a 10 ppm methylene blue solution was used as a model pollutant. The steam generation experiment was carried out for the dye solution instead of deionized water under a solar intensity of 5 kW m^{-2} and the resulting steam was condensed and analyzed using an HP-8453 UV-visible spectrophotometer.

Recycling study of the CC solar steam generation device

To evaluate the recyclability of the CC solar steam generation device, solar steam generation experiments were carried out for 10 cycles using a light density of 5 kW m^{-2}. Each cycle was carried out for 30 minutes and the device was cooled down to room temperature after each cycle by flushing cold DI water through the device.

Results and discussion

Fig. 1 displays the FT-IR spectra of the pure cotton and the CC fibers. The peak around 3325 cm^{-1} is attributed to the hydroxyl

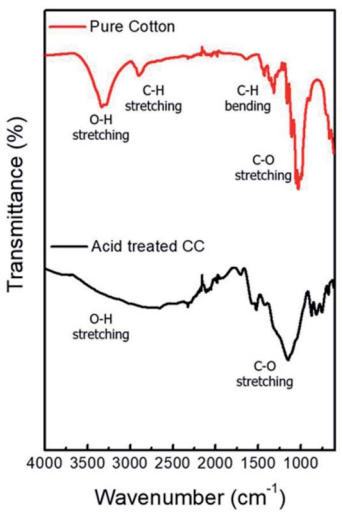

Fig. 1 FT-IR spectra of pure cotton and acid treated carbonized cotton (CC).

functional groups, which are present in abundance in pristine cotton fibers. Peaks at 2900, 1426 and 1054 cm^{-1} are ascribed to C–H stretching, CH_2 asymmetric bending and C–O stretching vibrations, respectively.[35] After the cotton is carbonized at 600 °C, most of the hydroxyl functional groups are removed and the resulting black carbonaceous fibers are hydrophobic due to the absence of polar functional groups. Since the hydrophobic CC cannot transport water to the evaporation surface, an acid treatment was performed to introduce oxygen functional groups such as hydroxyl and carboxylic groups to make the material partially hydrophilic. The peak for O–H stretching frequency of the acid-treated CC is not prominent and most likely overlapped with the C–H stretching peak. However, a broad peak ranging from 1000–1500 cm^{-1} is clearly visible which can be ascribed to overlapped peaks of C–H bending and C–O stretching frequencies.

XPS spectra were measured to evaluate the extent of oxidation in the CC fibers after the acid treatment. Fig. 2 displays the XPS data of the CC fibers before and after the acid treatment. After the acid treatment, an increase in the atomic percentage of oxygen is observed due to the addition of hydroxyl and carboxylic functional groups. Fig. 2(A) represents the XPS survey spectra of the CC fibers before and after acid treatment. The two peaks at 285.0 eV and 532.0 eV correspond to the C 1s and O 1s photoelectrons, respectively. An Auger peak is visible around 970 eV, which is responsible for the transition from L to K shell of oxygen, and is denoted as O KLL in the survey scan. The atomic percentage of oxygen before and after the acid treatment was calculated based on the peak area of the C 1s and O 1s peaks. Oxygen atomic percentage was found to increase from 6.3% to 24.8% after refluxing in 50% HNO_3 for one hour. High-resolution XPS spectra of the C 1s photoelectrons before and after the oxidation are displayed in Fig. 2(A) and (B), respectively. The dominant peak at 284.8 eV corresponds to C–C bond (diamond and graphitic type). A small amount of ethereal carbon (C–O and O–C–O) was also observed even before the acid treatment, which is probably coming from adventitious carbon deposited on the surface. After the acid treatment, a significant increase can be seen in peaks corresponding to C═O and O–C═O bonds (~287 eV and ~289 eV, respectively) due to the addition of carbonyl and carboxylic functional groups.[36,37] The addition of these polar functional groups effectively enhance the hydrophilicity of the CC fibers, which is vital in designing an efficient solar steam generation device.

SEM images of the pure cotton and the CC fibers are shown in Fig. 3. As shown in Fig. 3(A) and (B), the average diameter of pristine cotton (PC) fiber can range from 15 to 20 μm. However, after carbonization at 600 °C for 1 hour, the average diameter of the fiber decreased by about 50% due to the release of H_2O, CO and CO_2 during the carbonization process[38] (the weight of the cotton fiber also decreased by ~70% after carbonization). Also, during the heat treatment, most of the cotton fibers were cracked and opened probably due to the pressure build up from the evolved gases (Fig. 3(D)).

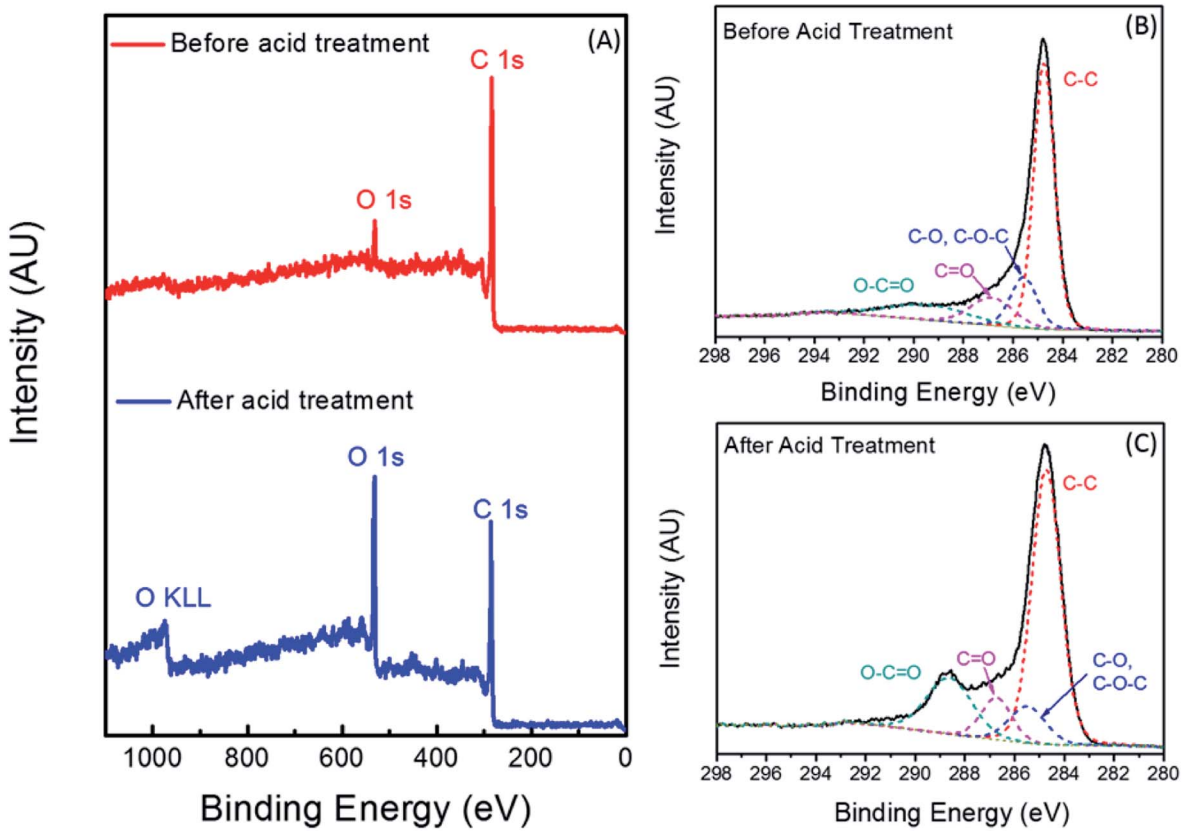

Fig. 2 (A) XPS survey spectra of CC before and after acid treatment. C 1s photoelectron spectrum of CC before (B) and after (C) acid treatment.

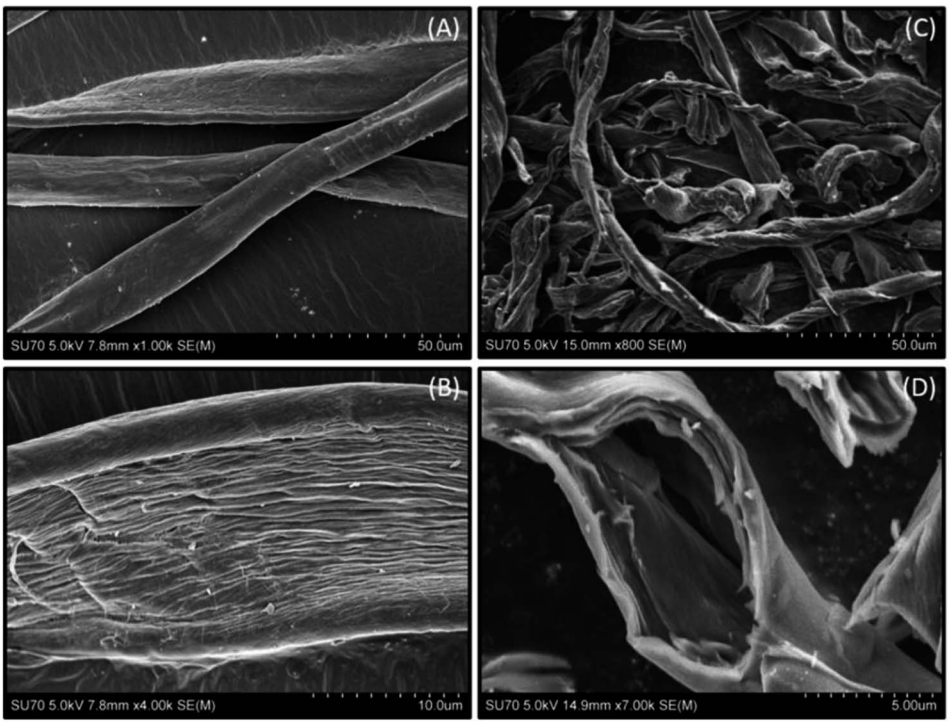

Fig. 3 SEM images of pristine cotton fibers ((A) and (B)) and carbonized cotton fibers ((C) and (D)).

The Raman spectrum of the carbonized cotton fibers is displayed in Fig. 4. The two peaks in the spectrum at 1350 cm^{-1} and 1590 cm^{-1} are assigned to the D and G bands, respectively.[31,32] The prominent G band ascertains that after carbonization at a higher temperature in an inert atmosphere (N_2), the cellulosic fibers were converted into sp^2 hybridized graphitic carbon.

Fig. 5 displays the reflectance and absorption spectra of the CC fibers. The low percentage reflectance in Fig. 5(A) is ascribed to the ultra-black color of the fibers. The absorption spectrum (Fig. 5 (B)) shows a broad profile with a percentage absorbance above 70% in the entire visible range of the solar spectrum, which is one of the key reasons to use carbonized materials as efficient photothermal energy converters.[39–42] The drop in the percentage absorbance by ~15% in the infrared region does not have a significant impact on the absorption of the CC fibers since the solar irradiance in the region after 800 nm is below ~0.6 W m^{-2} nm^{-1}.

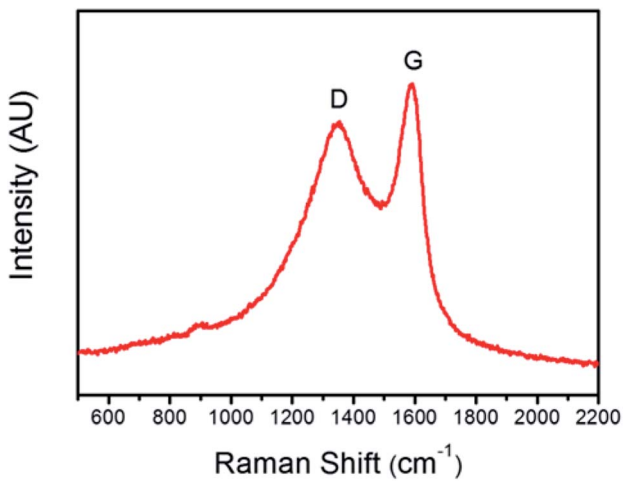

Fig. 4 Raman spectrum of carbonized cotton (CC) fibers.

The CC fibers with nearly full solar spectrum absorption, efficient photo-thermal conversion and low-cost could provide excellent alternatives to the high-cost plasmonic-based materials for solar water desalination.[7,8,20,43] However, because of the significant heat loss due to the large heat capacity of water, porous CC fibers that float on the surface of water are desired for efficient steam generation. To achieve this goal, we designed a new device to mount the CC fibers on low-density polymer foams to facilitate the buoyancy and floating capability of the fibers.[14,28,42,44] In addition to buoyancy, the low thermal conductivity of the polymer foams helps to efficiently localize the heat within the fibers and minimize the conductive heat loss. However, during the long-term steam generation process, the CC solar absorber and the polymer foam support can eventually start dissipating heat into bulk water due to the heat buildup. One way to address this issue is to reduce the contact surface area between bulk water and the CC solar absorber. Therefore, our design strategy involves elevating the CC irradiation surface above the evaporating water surface and providing a continuous flow of water to the CC solar absorber. This strategy is based on the natural mushroom design demonstrated recently to successfully minimize the conductive heat loss in solar desalination.[39]

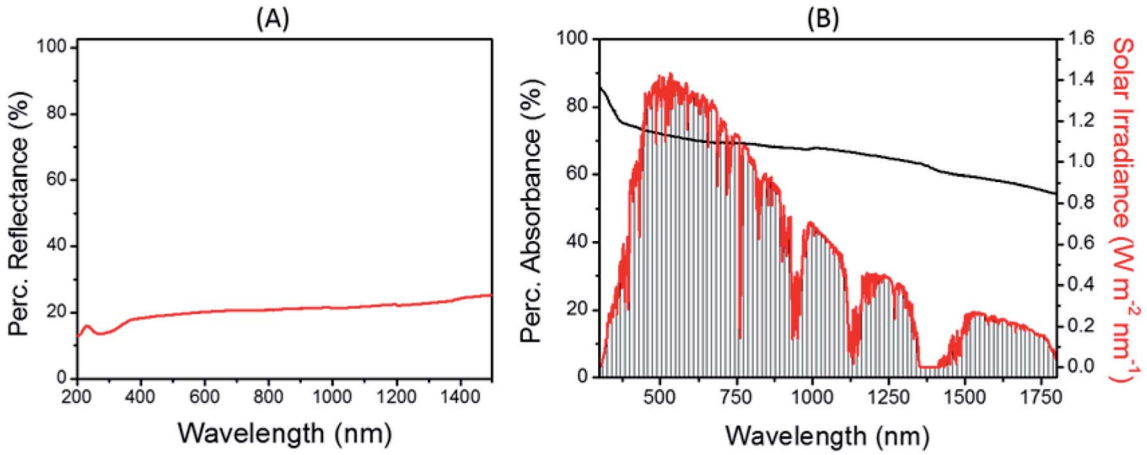

Fig. 5 Optical properties of the CC fibers. (A) Reflectance spectrum of CC and (B) Absorbance spectrum of CC in comparison with the solar irradiance.

To improve the durability and minimize the conductive heat loss to bulk water, the CC solar steam generation device is assembled according to the schematic representation shown in Fig. 6. In this design, the irradiation surface consists of a bilayer of functionalized carbonized cotton and pristine cotton fibers placed on a frame of low-density polyethylene foam. To feed water to the irradiation surface, a stalk made of pristine cotton fibers is utilized. The new design helps to solve some of the critical issues associated with the use of carbonized materials in solar steam generation such as material's shedding, conductive heat loss, and durability.[3,4,15]

To evaluate the performance of the CC solar steam generation device, the steam generation rates were measured at different solar intensities of 1 kW m^{-2} (1 sun), 5 kW m^{-2} (5 sun) and 8 kW m^{-2} (8 sun). The solar steam generation rate of the CC device was compared with a similar device using pristine cotton (PC) fibers as a solar absorber instead of the CC fibers and also with the steam rate of pure DI water in the absence of any solar absorber. The results presented in Fig. 7(A) and (B) show the normalized steam generation rates of the CC, PC and DI water samples at solar illumination of 1 sun and 8 sun, respectively (the results obtained at 5 sun are shown in Fig. S2, ESI†). It is clear that the CC device exhibits significantly higher evaporation rates compared to the PC device at both solar intensities of 1 and 8 sun as shown in Fig. 7(A) and (B), respectively. The solar evaporation rates of the CC device are 0.9, 6.4 and 10.9 kg m^{-2} h^{-1} at solar illumination intensities of 1, 5 and 8 sun, respectively. For comparison, the rates of the PC device are 0.4, 1.7 and 2.4 kg m^{-2} h^{-1} at the solar intensities of 1, 5 and 8 sun, respectively. Therefore, the solar evaporation rate of the CC device at 8 sun is almost 5 times higher than that of the PC devise mainly due to the high solar absorption of the CC fibers as compared to the white color PC fibers which reflect solar light efficiently. In spite of the lack of solar absorption, the steam generation rate of the PC fibers is higher than that of DI water since the hydrophilic fibrous structure enhances water surface evaporation.

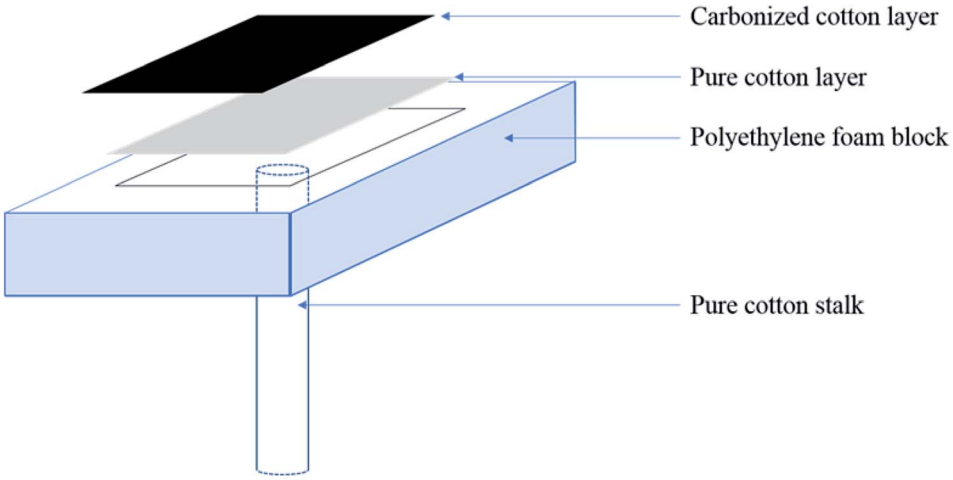

Fig. 6 Schematic representation of the CC solar steam generation device.

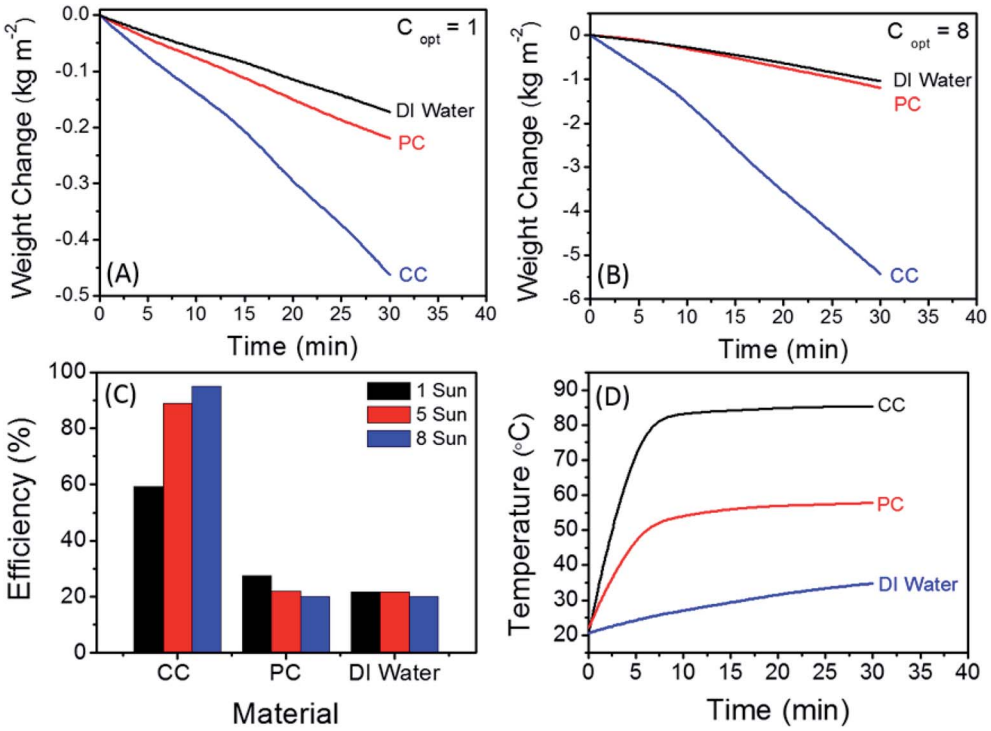

Fig. 7 Solar steam generation data for carbonized cotton (CC), pristine cotton (PC) and DI water at solar intensities of (A) 1 kW m^{-2} (1 sun) and (B) 8 kW m^{-2} (8 sun). (C) The solar-to-vapor evaporation efficiency of CC, PC and DI water at 1, 5 and 8 sun solar illuminations. (D) Surface temperature profiles of CC, PC and DI water at 8 sun solar illumination.

The solar-to-vapor efficiency is calculated based on the equation $\eta_{TH} = \dot{m}h_{LV}/C_{opt}q_i$ where η_{TH} is the thermal efficiency, $\dot{m}$ is the mass flux in g m^{-2} h^{-1}, h_{LV} is the total enthalpy for the phase change from liquid to vapor in J, C_{opt} is the optical concentration (number of suns) and q_i is the nominal solar intensity defined as 1 kW m^{-2}.[28,30,45] As shown in Fig. 7(C), the calculated solar-to-vapor efficiencies of the CC device are 59.2, 88.7 and 94.9% at solar intensities of 1, 5 and 8 sun, respectively. The calculated efficiency at 8 sun is among the highest values reported for photothermal energy conversion materials used for solar water desalination as demonstrated by the date displayed in Table 1.

The surface temperature profiles of the CC and PC devices and DI water during the operation at 8 sun of solar intensity are plotted in Fig. 7(D). For the CC device, the surface temperature increased from room temperature to 80 °C within 5 min a steady state of ~85 °C is reached after 15 min. However, the surface temperature of the PC device only reached 51 °C after 5 min and its equilibrium temperature was only ~57 °C. Due to the special design of the CC device, the heat loss to bulk water is greatly

Table 1 Solar water evaporation rates and efficiencies of various photothermal conversion materials reported in literature

Photo thermal conversion materials	Number of suns	Evaporation efficiency (%)	Evaporation rate (kg m^{-2} h^{-1})	References
Functionalized carbonized cotton (CC) fibers	1	59.2%	0.9	This work
	5	88.7%	6.4	
	8	94.9%	10.9	
rGO-MCE	1	60.0	—	46
P-wood	10	85%	11.8	34
C foam-graphite	10	85%	—	23
Natural wood with artificial channel-array	1	75.1%	1.04	47
CNT-modified flexible wood	10	81.0%	11.22	48
Plasmonic wood	10	85.0%	11.8	34
BNC-RGO	10	83.0%	11.8	49
rGO-PU	10	81.0%	11.24	31
Au/Ag-PFC fibers	8	94.3%	11.3	8
Graphene oxide-wood	12	82.8%	10.08	50
PDMS-wood	6	78.0	6.4	51
Graphite-wood	10	89.0%	12.31	52
Au/Ag-PGPU foams	8	96.5%	11.34	7

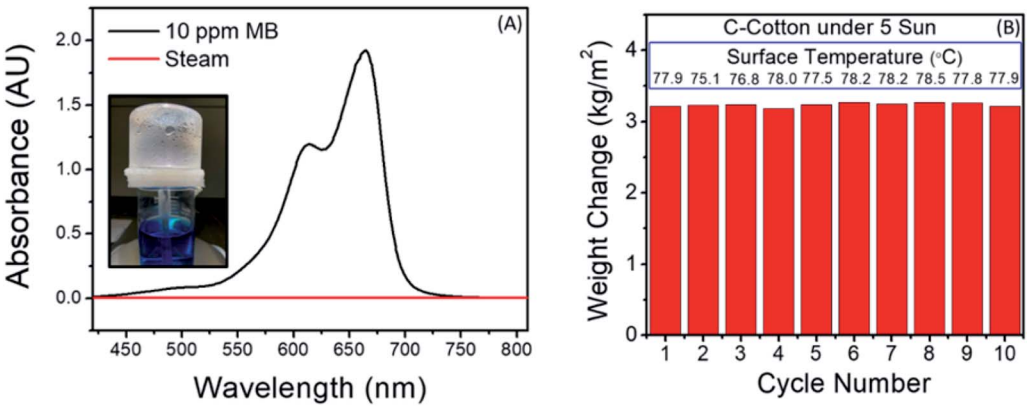

Fig. 8 (A) UV-Vis spectra of 10 ppm MB dye solution and condensed steam sample (a photograph of the steam collection setup is shown in the inset). (B) Recyclability test of the CC device during 10 cycles of constant solar irradiation under the solar intensity of 5 sun.

minimized. At all solar intensities, the temperature increment in bulk water was less than 1 °C. Conduction heat loss is considered one of the main contributors to energy loss in solar steam generation devices. Conduction heat loss can be quantified using Fourier's law where the conductive heat flux j is given by $j = \kappa\,\Delta T/L$ where κ is the thermal conductivity of the cotton stalk (0.026 W m^{-1} K^{-1}) and $\Delta T/L$ is the temperature gradient across the cotton stalk. In our CC device, the pure cotton stalk was about 5 cm in length and 0.8 cm in diameter. Therefore, the calculated conductive heat flux is around 6.3 W m^{-2}, which is about 0.6% heat loss at 1 sun and even lower at 8 sun (~0.4%).[53] Moreover, the frame of the CC solar steam generation device is made of polyethylene foam which has a low thermal conductivity (~0.04 W m^{-1} K^{-1})[53] and therefore, it helps to confine the heat within the irradiation area of the CC fibers. The percentage conductive heat loss of the CC device (~0.4–0.6%) is significantly lower than the 2.2% calculated for the plasmonic functionalized cotton fibers where the irradiation area was in direct contact with bulk water.[7,8] Thus, it is palpable that the novel low-cost design of the CC solar steam generation device effectively reduces the heat loss to bulk water.

Another application of the CC device is to extract pure water from contaminated and wastewater. Fig. 8(A) displays the UV-Vis spectra of the 10 ppm methylene blue (MB) dye solution and the condensed water of the steam generated from the dye solution under solar irradiation at 5 sun using the CC device. As expected, a complete removal of the dye from the condensed steam is confirmed.

Fig. 8(B) displays the recyclability data of the CC device during 10 steam generation cycles under the solar intensity of 5 sun. The average normalized steam generation rate after 10 cycles is 3.2 ± 0.03 kg m^{-2}, which demonstrates the excellent stability and reusability of the CC fibers for solar steam generation.

Conclusions

In conclusion, we designed and developed metal-free, low weight and cost effective functionalized carbonized cotton (CC) fibers for efficient solar water desalination and wastewater treatment. The CC fibers with nearly full solar spectrum absorption, efficient photo-thermal conversion and low-cost could provide excellent alternatives to the high-cost plasmonic-based materials for solar water desalination. The CC fibers are used as an irradiation surface placed on a low-density and low thermal conductivity polyethylene foam that floats on the surface of seawater, which helps to efficiently localize the heat within the fibers and minimize the conductive heat loss.

The CC solar steam generation device exhibits average water evaporation rates of 0.9, 6.4 and 10.9 kg m^{-2} h^{-1} with impressive solar-to-vapor efficiencies of 59.2, 88.7 and 94.9% under 1, 5 and 8 sun illumination, respectively. Moreover, the device displays excellent durability showing stable evaporation rates over 10 steam generation cycles under 5 sun of solar intensity. Furthermore, the applicability of the CC device for the removal of organic dyes from contaminated water through the solar steam generation is also demonstrated. The low-cost, simple design, high solar thermal evaporation efficiency, excellent stability and long-time durability make this CC device a perfect candidate for applications in seawater desalination and wastewater treatment by solar-steam generation.

Conflicts of interest

The authors declare that they have no conflict of interest.

Acknowledgements

This work was supported by the National Science Foundation (CHE-1463989) and the Virginia Center for Innovative Technology VA-CIT CRCF Award # MF17-046-En. We thank Professor Ümit Özgür (VCU Department of Electrical and Computer Engineering) for his help in the use of the solar simulator. We thank Dr Indika U. Arachchige (VCU Department of Chemistry) for his help in the optical characterization of the materials.

References

1 M. M. Mekonnen and A. Y. Hoekstra, *Sci. Adv.*, 2016, **2**, e1500323.
2 M. Elimelech and W. A. Phillip, *Science*, 2011, **333**, 712–717.
3 M. Chandrashekara and A. Yadav, *Renewable Sustainable Energy Rev.*, 2017, **67**, 1308–1330.
4 H. Sharon and K. Reddy, *Renewable Sustainable Energy Rev.*, 2015, **41**, 1080–1118.
5 L. Zhu, M. Gao, C. K. N. Peh and G. W. Ho, *Nano Energy*, 2019, **57**, 507–518.
6 X. Wu, G. Y. Chen, G. Owens, D. Chu and H. Xu, *Mater. Today Energy*, 2019, **12**, 277–296.
7 F. S. Awad, H. D. Kiriarachchi, K. M. AbouZeid, U. Ozgur and M. S. El-Shall, *ACS Appl. Energy Mater.*, 2018, **1**, 976–985.
8 H. D. Kiriarachchi, F. S. Awad, A. A. Hassan, J. A. Bobb, A. Lin and M. S. El-Shall, *Nanoscale*, 2018, **10**, 18531–18539.
9 J. He, Y. Fan, C. Xiao, F. Liu, H. Sun, Z. Zhu, W. Liang and A. Li, *Compos. Sci. Technol.*, 2021, **204**, 108633.
10 Y. Wang, X. Wu, T. Gao, Y. Lu, X. Yang, G. Y. Chen, G. Owens and H. Xu, *Nano Energy*, 2021, **79**, 105477.
11 Y. Zou, P. Yang, L. Yang, N. Li, G. Duan, X. Liu and Y. Li, *Polymer*, 2021, **217**, 123464.
12 J. Feng, B. Bai, L. Yang, N. Hu and H. Wang, *Mater. Chem. Phys.*, 2021, **271**, 124904.
13 Y. Liu, X. Wang and H. Wu, *Chem. Eng. J.*, 2017, **309**, 787–794.
14 O. Neumann, C. Feronti, A. D. Neumann, A. Dong, K. Schell, B. Lu, E. Kim, M. Quinn, S. Thompson and N. Grady, *Proc. Natl. Acad. Sci. U. S. A.*, 2013, **110**, 11677–11681.
15 V. S. Reddy, S. Kaushik, K. Ranjan and S. Tyagi, *Renewable Sustainable Energy Rev.*, 2013, **27**, 258–273.
16 X. Ming, A. Guo, G. Wang and X. Wang, *Sol. Energy Mater. Sol. Cells*, 2018, **185**, 333–341.
17 D. Ding, W. Huang, C. Song, M. Yan, C. Guo and S. Liu, *Chem. Commun.*, 2017, **53**, 6744–6747.
18 X. Yang, Y. Yang, L. Fu, M. Zou, Z. Li, A. Cao and Q. Yuan, *Adv. Funct. Mater.*, 2018, **28**, 1704505.
19 L. Zhou, Y. Tan, J. Wang, W. Xu, Y. Yuan, W. Cai, S. Zhu and J. Zhu, *Nat. Photonics*, 2016, **10**, 393–398.
20 M. Wang, P. Wang, J. Zhang, C. Li and Y. Jin, *ChemSusChem*, 2019, **12**, 467–472.
21 M. Chen, Y. Wu, W. Song, Y. Mo, X. Lin, Q. He and B. Guo, *Nanoscale*, 2018, **10**, 6186–6193.
22 L. Ren, X. Yi, Z. Yang, D. Wang, L. Liu and J. Ye, *Nano Lett.*, 2021, **21**, 1709–1715.
23 H. Ghasemi, G. Ni, A. M. Marconnet, J. Loomis, S. Yerci, N. Miljkovic and G. Chen, *Nat. Commun.*, 2014, **5**, 1–7.
24 Z. Yin, H. Wang, M. Jian, Y. Li, K. Xia, M. Zhang, C. Wang, Q. Wang, M. Ma and Q.-s. Zheng, *ACS Appl. Mater. Interfaces*, 2017, **9**, 28596–28603.
25 D. Wu, C. Du and C. Huang, *Appl. Therm. Eng.*, 2021, 117238.
26 A. Wei, K. Cui, P. Wang, Y. Gu, X. Wang, X. Mu, Y. Tian, J. Zhou, Z. Sun and Y. Chen, *Sol. RRL*, 2021, **5**, 2000782.
27 Y. Sun, Z. Zhao, G. Zhao, L. Wang, D. Jia, Y. Yang, X. Liu, X. Wang and J. Qiu, *Carbon*, 2021, **179**, 337–347.
28 X. Li, W. Xu, M. Tang, L. Zhou, B. Zhu, S. Zhu and J. Zhu, *Proc. Natl. Acad. Sci. U. S. A.*, 2016, **113**, 13953–13958.
29 X. Wang, G. Ou, N. Wang and H. Wu, *ACS Appl. Mater. Interfaces*, 2016, **8**, 9194–9199.
30 X. Hu, W. Xu, L. Zhou, Y. Tan, Y. Wang, S. Zhu and J. Zhu, *Adv. Mater.*, 2017, **29**, 1604031.
31 G. Wang, Y. Fu, A. Guo, T. Mei, J. Wang, J. Li and X. Wang, *Chem. Mater.*, 2017, **29**, 5629–5635.
32 P. Zhang, J. Li, L. Lv, Y. Zhao and L. Qu, *ACS Nano*, 2017, **11**, 5087–5093.
33 J. Fang, J. Liu, J. Gu, Q. Liu, W. Zhang, H. Su and D. Zhang, *Chem. Mater.*, 2018, **30**, 6217–6221.
34 M. Zhu, Y. Li, F. Chen, X. Zhu, J. Dai, Y. Li, Z. Yang, X. Yan, J. Song and Y. Wang, *Adv. Energy Mater.*, 2018, **8**, 1701028.
35 L.-L. Xu, M.-X. Guo, S. Liu and S.-W. Bian, *RSC Adv.*, 2015, **5**, 25244–25249.
36 B. Li, F. Dai, Q. Xiao, L. Yang, J. Shen, C. Zhang and M. Cai, *Energy Environ. Sci.*, 2016, **9**, 102–106.
37 M. Sevilla and A. B. Fuertes, *Carbon*, 2009, **47**, 2281–2289.
38 M. Zhang, C. Wang, H. Wang, M. Jian, X. Hao and Y. Zhang, *Adv. Funct. Mater.*, 2017, **27**, 1604795.
39 N. Xu, X. Hu, W. Xu, X. Li, L. Zhou, S. Zhu and J. Zhu, *Adv. Mater.*, 2017, **29**, 1606762.
40 G. Xue, K. Liu, Q. Chen, P. Yang, J. Li, T. Ding, J. Duan, B. Qi and J. Zhou, *ACS Appl. Mater. Interfaces*, 2017, **9**, 15052–15057.
41 Y. Chen, Y. Shi, H. Kou, D. Liu, Y. Huang, Z. Chen and B. Zhang, *ACS Sustainable Chem. Eng.*, 2019, **7**, 2911–2915.
42 Y. Liu, J. Chen, D. Guo, M. Cao and L. Jiang, *ACS Appl. Mater. Interfaces*, 2015, **7**, 13645–13652.
43 A. F. Zedan, S. Moussa, J. Terner, G. Atkinson and M. S. El-Shall, *ACS Nano*, 2013, **7**, 627–636.
44 J. Yang, Y. Pang, W. Huang, S. K. Shaw, J. Schiffbauer, M. A. Pillers, X. Mu, S. Luo, T. Zhang and Y. Huang, *ACS Nano*, 2017, **11**, 5510–5518.
45 M. Zhu, Y. Li, F. Chen, X. Zhu, J. Dai, Y. Li, Z. Yang, X. Yan, J. Song, Y. Wang, E. Hitz, W. Luo, M. Lu, B. Yang and L. Hu, *Adv. Energy Mater.*, 2018, **8**, 1701028.
46 G. Wang, Y. Fu, X. Ma, W. Pi, D. Liu and X. Wang, *Carbon*, 2017, **114**, 117–124.
47 Y. Kuang, C. Chen, S. He, E. M. Hitz, Y. Wang, W. Gan, R. Mi and L. Hu, *Adv. Mater.*, 2019, **31**, 1900498.
48 C. Chen, Y. Li, J. Song, Z. Yang, Y. Kuang, E. Hitz, C. Jia, A. Gong, F. Jiang and J. Zhu, *Adv. Mater.*, 2017, **29**, 1701756.
49 Q. Jiang, L. Tian, K. K. Liu, S. Tadepalli, R. Raliya, P. Biswas, R. R. Naik and S. Singamaneni, *Adv. Mater.*, 2016, **28**, 9400–9407.
50 K.-K. Liu, Q. Jiang, S. Tadepalli, R. Raliya, P. Biswas, R. R. Naik and S. Singamaneni, *ACS Appl. Mater. Interfaces*, 2017, **9**, 7675–7681.
51 S. He, C. Chen, Y. Kuang, R. Mi, Y. Liu, Y. Pei, W. Kong, W. Gan, H. Xie and E. Hitz, *Energy Environ. Sci.*, 2019, **12**, 1558–1567.
52 T. Li, H. Liu, X. Zhao, G. Chen, J. Dai, G. Pastel, C. Jia, C. Chen, E. Hitz and D. Siddhartha, *Adv. Funct. Mater.*, 2018, **28**, 1707134.
53 O. Almanza, M. A. Rodríguez-Pérez and J. A. De Saja, *J. Polym. Sci., Part B: Polym. Phys.*, 2004, **42**, 1226–1234.